Pacific Interdecadal Climate Variability: Linkages between the Tropics and the North Pacific during Boreal Winter since 1900

CLARA DESER, ADAM S. PHILLIPS, AND JAMES W. HURRELL

Climate and Global Dynamics Division, NCAR, Boulder, Colorado

(Manuscript received 8 August 2003, in final form 20 February 2004)

ABSTRACT

This study examines the tropical linkages to interdecadal climate fluctuations over the North Pacific during boreal winter through a comprehensive and physically based analysis of a wide variety of observational datasets spanning the twentieth century. Simple difference maps between epochs of high sea level pressure over the North Pacific (1900–24 and 1947–76) and epochs of low pressure (1925–46 and 1977–97) are presented for numerous climate variables throughout the tropical Indo-Pacific region, including rainfall, cloudiness, sea surface temperature (SST), and sea level pressure. The results support the notion that the Tropics play a key role in North Pacific interdecadal climate variability. In particular, SST anomalies in the tropical Indian Ocean and southeast Pacific Ocean, rainfall and cloudiness anomalies in the vicinity of the South Pacific convergence zone, stratus clouds in the eastern tropical Pacific, and sea level pressure differences between the tropical southeast Pacific and Indian Oceans all exhibit prominent interdecadal fluctuations that are coherent with those in sea level pressure over the North Pacific. The spatial patterns of the interdecadal tropical climate anomalies are compared with those associated with ENSO, a predominantly interannual phenomenon; in general, the two are similar with some differences in relative spatial emphasis. Finally, a published 194-yr coral record in the western tropical Indian Ocean is shown to compare favorably with the twentieth-century instrumental records, indicating the potential for extending knowledge of tropical interdecadal climate variability to earlier time periods.

1. Introduction

Numerous studies have documented interdecadal variations in climate over the North Pacific, including Trenberth and Hurrell (1994), Mantua et al. (1997, hereafter M97), Minobe (1997), Zhang et al. (1997), Dettinger et al. (2000), Chao et al. (2000), and Mantua and Hare (2002). These interdecadal climate fluctuations are characterized by changes in the intensity of the large-scale atmospheric circulation over the North Pacific during winter, with impacts upon physical and biological conditions in the North Pacific Ocean and consequences for climate downstream over North America, including air temperature, precipitation, streamflow, and vegetation (Cayan et al. 2001). An index of the strength of the wintertime atmospheric circulation over the North Pacific is shown in Fig. 1 for the period 1899–2003. This ''North Pacific Index'' (NPI; see Trenberth and Hurrell 1994) is the area-averaged sea level pressure (SLP) for the region 30°–65°N, 160°–140°W. Negative values correspond to a deeper-than-normal Aleutian low pressure system, accompanied by enhanced westerly winds across the central North Pacific and strengthened southerly (northerly) flow over the eastern (western) North Pacific; opposite conditions obtain for positive values. The NPI also provides a proxy record of the Pacific–North American (PNA) teleconnection pattern evident in the middle troposphere (Trenberth and Hurrell 1994). A striking feature of the NPI is the occurrence of extended periods, two to three decades in duration, with predominantly positive (1900–24 and 1947–76) or negative values (1925–46 and 1977–2003). In addition to the interdecadal fluctuations associated with the phase transitions in 1925, 1947, and 1977, the NPI also exhibits considerable high-frequency variability: approximately 75% of the variance of the NPI occurs at periods shorter than 20 yr (not shown).

What are the origins of interdecadal fluctuations in the NPI? Several hypotheses have been proposed, including coupled ocean–atmosphere interactions within the North Pacific (Latif and Barnett 1996; Robertson 1996) and with extensions to the tropical Pacific via an atmospheric bridge (Barnett et al. 1999); air–sea interaction within the subtropical Pacific, with atmospheric teleconnections to the North Pacific as a by-product (Knutson and Manabe 1998; Kleeman et al. 1999; McPhaden and Zhang 2002; Nonaka et al. 2002; Vimont et al. 2001; Liu et al. 2002); extratropical–tropical interactions via an equatorward subsurface oceanic pathway and a return atmospheric bridge (Gu and Philander 1997; Deser et al. 1996; Schneider et al. 1999); and

Corresponding author address: Dr. Clara Deser, Climate and Global Dynamics Division, NCAR, P.O. Box 3000, Boulder, CO 80307.
E-mail: cdeser@ucar.edu

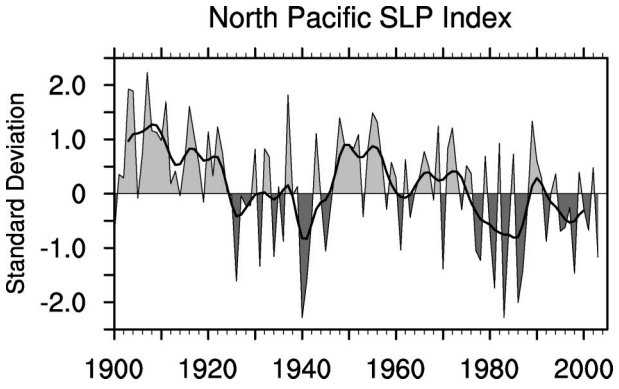

FIG. 1. The NPI from 1900 to 2003, normalized by its std dev (2.3 hPa). The NPI is defined as the winter mean (Dec–Mar) SLP anomaly averaged over the region 30°–65°N, 160°–140°W. The shaded curve is the raw time series and the thick black curve is a low-pass-filtered version using a weighted seven-point running mean.

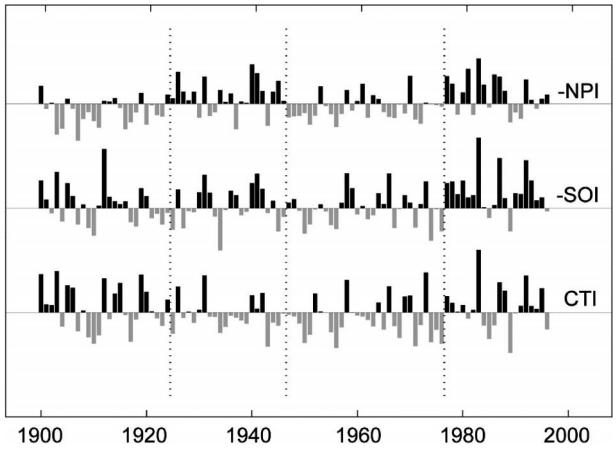

FIG. 2. The (top) inverted NPI, (middle) inverted SOI, and (bottom) eastern equatorial Pacific SST (the CTI) during 1900–96, normalized by their respective std devs. The dashed vertical lines denote regime transitions identified on the basis of the NPI (1925, 1947, and 1977). This figure is reproduced from M97.

climate noise due to the integrating effect of stochastic atmospheric variability by the North Pacific Ocean mixed layer (Pierce et al. 2001; Newman et al. 2003) and the thermocline (Frankignoul et al. 2000). Note that the Tropics play an active role in some theories but not in others.

What do observational studies indicate about the role of the Tropics in North Pacific interdecadal climate variability? Many have shown that the 1977 climate transition in the North Pacific is evident in the tropical Pacific where it resembles the pattern associated with the warm phase of the El Niño–Southern Oscillation (ENSO) phenomenon (e.g., Nitta and Yamada 1989; Trenberth and Hurrell 1994; Graham et al. 1994; Houghton et al. 1996; M97; Zhang et al. 1997; Garreaud and Battisti 1999). Less is known about the tropical signature of the earlier climate transitions in 1925 and 1947. Figure 2, reproduced from M97, compares the NPI with two canonical indices of ENSO: an equatorial Pacific sea surface temperature (SST) index (the average of SST anomalies in the region 6°N–6°S, 180°–90°W) from which the global mean SST anomalies have been subtracted and a Southern Oscillation index (SOI) [the SLP difference between the tropical Indian/western Pacific and the remaining oceanic areas (see M97 for details)]. While the 1977 transition is evident in both ENSO records, the 1925 and 1947 shifts are not as clear. For example, the 1925 transition is absent from the SOI (which remains predominantly positive throughout the first half of the twentieth century), and the 1947 shift is absent from the SST index. Furthermore, the trend of the SST index during the first half of the twentieth century is in the opposite sense to that of the NPI. These discrepancies raise the question, Was the 1977 transition unique in terms of its connection to the tropical Pacific as measured by the canonical ENSO indices, or are there other regions of the Tropics that exhibit a more consistent linkage to the NPI during the twentieth century?

Preliminary evidence for a robust tropical connection was presented by Minobe (1997), who showed that annually averaged SST anomalies in the tropical Indian Ocean vary coherently with the NPI on interdecadal time scales. A more systematic investigation of the relationship between the North Pacific and the Tropics on time scales longer than ~6 yr was presented by Zhang et al. (1997). They used linear regression analysis to document the annually averaged SST and SLP anomaly patterns associated with the dominant mode of global SST variability (a structure that resembles the 1977 climate transition) after the effects of global warming and interannual ENSO fluctuations are removed. They characterized the patterns as ''ENSO-like'' in view of their general similarity to those associated with the ENSO cycle. Due to the statistical nature of their approach, Zhang et al.'s analysis provides a general description of Pacific low-frequency variability weighted toward the data-rich post–World War II period; it does not provide a specific description of each of the climate transitions individually.

In this study, we revisit the issue of tropical linkages to North Pacific interdecadal climate variability through a comprehensive and physically based analysis of a wide variety of observational datasets spanning the twentieth century. As mentioned earlier, elucidating the role of the Tropics is important from the standpoint of providing guidance for mechanistic studies of Pacific interdecadal climate variability. We present simple difference maps between epochs of high (1900–24 and 1947–76) and low (1925–46 and 1977–97) NPI for numerous climate variables in the tropical Indo-Pacific region, including SST, SLP, air temperature, precipitation, and cloudiness, emphasizing physical consistency among the various climatic parameters to build confidence in the results. Comparing the three epoch differences (1900–24 minus 1925–46; 1947–76 minus 1925–46; and 1947–76 minus 1977–97) allows us to assess those

features that are common to all three and those that are specific to a single case. All of the analyses are for the boreal winter season, December–March, unless noted otherwise. This choice is dictated by the season of strongest atmospheric circulation variability over the North Pacific (cf. Trenberth and Hurrell 1994) and established physical mechanisms for atmospheric teleconnections forced by deep convection in the Tropics (cf. Trenberth et al. 1998; Alexander et al. 2002). A suite of selected time series for key regions and climate parameters is also developed to further characterize and synthesize the tropical interdecadal variability that is coherent with the NPI. Finally, we compare the patterns of tropical climate anomalies on interannual (ENSO) and interdecadal time scales, as in Garreaud and Battisti (1999; note that their analysis is limited to the post-1958 period and considers only annual averages). As far as we are aware, our study is the first to examine, in a comprehensive and systematic manner, the tropical Indo-Pacific climate anomalies associated with interdecadal variations in the NPI during boreal winter.

The paper is organized as follows: The datasets and analysis procedures are described in section 2. Epoch difference maps associated with the climate transitions in 1925, 1947, and 1977 are presented in section 3 along with selected regional time series. The results are summarized and discussed in section 4, including a comparison to ENSO and a 194-yr paleoclimate reconstruction based upon a tropical Indian Ocean coral record (Cole et al. 2000).

2. Data and methods

Our strategy is to examine a suite of independent climate variables for collective evidence of coherent low-frequency variability over the Indo-Pacific sector. We examine the period 1900–97 for all variables, although some datasets may nominally extend further back in time and some may be updated beyond 1997. Our choice of 1900 as the starting year for the analysis is based upon data coverage considerations (cf. Woodruff et al. 1987).

For SST, we make use of two archives: the Comprehensive Ocean–Atmosphere Data Set (COADS; Woodruff et al. 1987) and the Lamont-Doherty Earth Observatory analyses (Kaplan et al. 1998). The COADS archive contains monthly data assembled into 2° latitude $\times$ 2° longitude grid squares over the global oceans dating back to 1854 with a minimum of processing (e.g., standard quality control procedures but no filling in of missing data). The Kaplan et al. dataset contains monthly data on a 5° latitude $\times$ 5° longitude grid over the global oceans dating back to 1871 with substantially more processing than in COADS. The input data to the Kaplan et al. analyses are from the Met Office historical SST dataset (Folland and Parker 1995), which are similar to the COADS except that additional corrections have been applied to empirically account for the artificial rise in SST around 1940 associated with the change in measurement technique from bucket to engine-intake temperatures. In the Kaplan et al. analyses, missing grid squares have been filled in using an (empirical orthogonal function) EOF-based technique. While this dataset has the advantage of increased spatial coverage and smoother fields than in the COADS, it may also introduce climate signals into areas devoid of observations or with limited data coverage. We have verified that our findings based upon the Kaplan et al. dataset are confirmed by the COADS.

For air temperature, we use the University of East Anglia's Climate Research Unit (CRU) dataset (Jones 1994), archived on a 5° $\times$ 5° latitude–longitude grid based upon land stations and ships of opportunity. For SLP, we make use of the COADS and an updated version of Trenberth and Paolino (1980). The latter is based upon daily historical analyses for the Northern Hemisphere poleward of 20°N on a 5° $\times$ 5° latitude–longitude grid. For precipitation, we use the gridded dataset (2.5° latitude $\times$ 3.75° longitude) from the University of East Anglia's CRU (Hulme et al. 1998) based upon land station records. We also make use of total cloud amount from the COADS as a proxy for precipitation over the oceans in regions where rainfall-producing cloud systems occur. (All datasets are available online at http://www.cgd.ucar.edu/cas/guide/.)

We formed monthly anomalies by subtracting the long-term monthly means from each calendar month's mean. Winter (December–March) means were computed from the monthly anomalies, requiring a minimum of 1 month to define a winter average. To improve the readability of the maps shown for COADS variables (SLP and cloudiness) and precipitation, linear interpolation (across gaps not exceeding three points in latitude and five points in longitude) and weighted binomial smoothing (three points in latitude and nine points in longitude) were applied. All regional time series are based on the raw (uninterpolated and unsmoothed) data. We formed epoch difference maps requiring a minimum of 20% of the years within each period to have observations. All data were detrended prior to computation of the epoch difference maps. The statistical significance of the epoch difference values is assessed by means of a Student's *t* test taking into account serial correlation (Zwiers and von Storch 1995; maps of the Student's *t* values may be viewed online at http://www.cgd.ucar.edu/~cdeser/PDVsupfig.html for each epoch difference field). When discussing the epoch difference maps, we emphasize mainly those features that are significant at the 95% confidence level.

Simple linear correlation analysis is used to quantify the relationship between two time series. The statistical significance of the resulting correlation coefficient is assessed according to a one-tailed Student's *t* test taking into account temporal autocorrelation following Trenberth (1984). A correlation coefficient that exceeds 0.36 in absolute value is significantly different from 0 at the

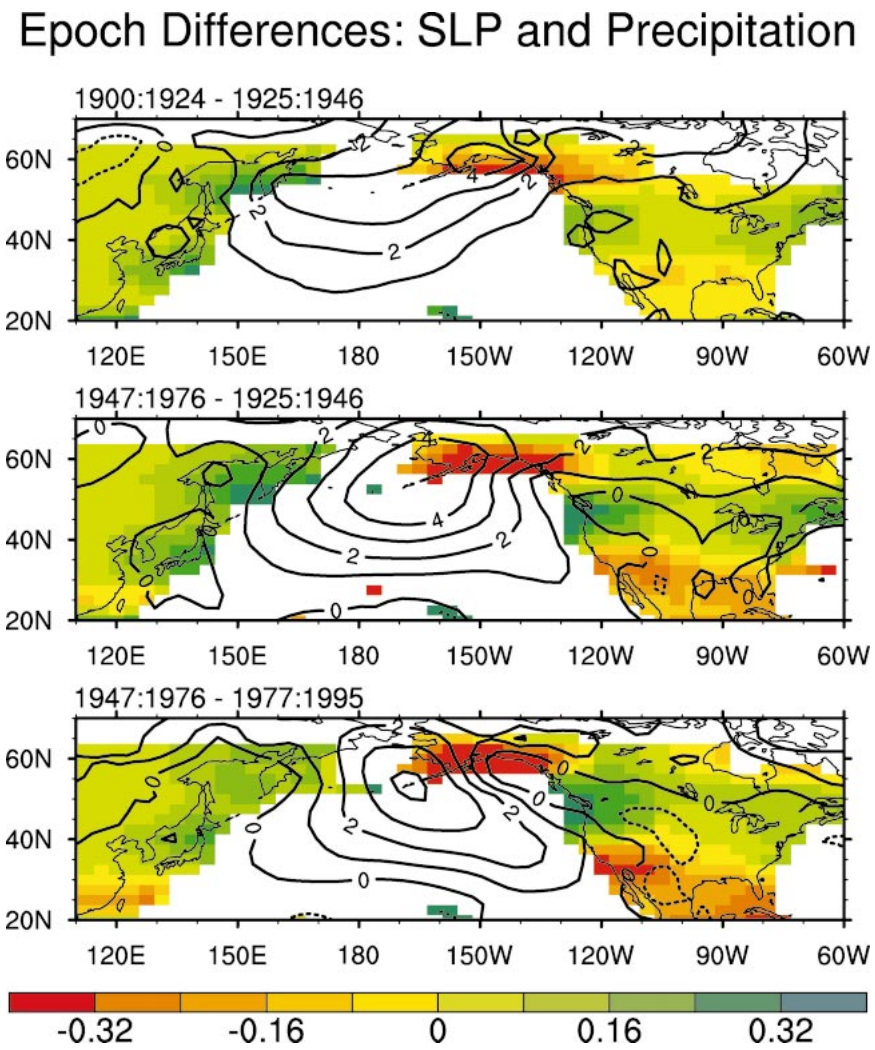

FIG. 3. Epoch difference maps of winter SLP (contours) and land precipitation (color shading) for high-minus-low NPI regimes (years as indicated above each panel). The contour interval for SLP is 1 hPa and negative contours are dashed. The precipitation scale (color bar at bottom of figure) is in units of mm day^{-1}.

95% confidence level for data that have been temporally smoothed with a three-point binomial filter. All of the correlation coefficients cited in this study exceed this value unless otherwise noted and are maximum at 0 lag.

3. Results

a. Extratropics

Atmospheric circulation variations associated with the NPI have important consequences for climate over the North Pacific and adjacent continents, as discussed in the introduction. Figure 3 shows epoch difference maps of winter SLP and precipitation for high-minus-low NPI regimes: 1900–24 minus 1925–46; 1947–76 minus 1925–46; and 1947–76 minus 1977–97. As expected, positive SLP values extend over a broad region of the North Pacific in all three epoch difference maps, with maximum values ~4 hPa in the vicinity of the Aleutian Islands. Some differences are also apparent, particularly in the orientation of the anomalous ridge over the eastern North Pacific, which shows a pronounced southeastward extension in the most recent epoch difference map compared to the early one. The precipitation fields are similar for the three epoch differences, with positive values along the Asian coast (Japan and the Kamchatka peninsula), negative values in southern Alaska and the southwestern United States, and positive values over the Pacific Northwest. The similarity among the maps, particularly the first and last, which contain no data in common, provides support for the robustness of the precipitation patterns. The banded structure over North America is similar to that documented in Dettinger et al. (2000) based upon station records of precipitation and streamflow. The precipita-

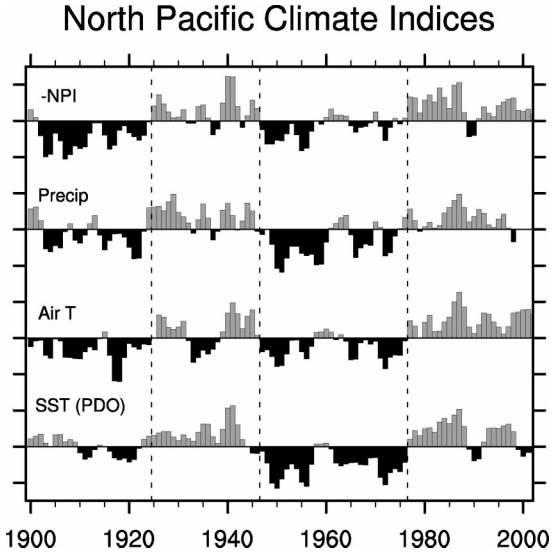

FIG. 4. Selected regional climate records over the North Pacific and adjacent continents during 1899–2002 (1899–1998 for precipitation): the inverted NPI, the winter precipitation difference between coastal Alaska and Japan, winter surface air temperature anomalies over northwestern Canada and Alaska, and the leading PC time series of monthly SST anomalies over the North Pacific from M97 averaged for the winter–spring season (see text for precise definitions). All records are normalized and smoothed with a three-point binomial filter. Each tick mark on the ordinate represents 1 std dev.

tion patterns are understandable in the context of the large-scale atmospheric circulation changes. For example, a weak Aleutian low (anomalously high SLP) is accompanied by reduced low-level southerly flow over the eastern North Pacific that decreases the moisture flux into coastal Alaska, consistent with the precipitation response. Similarly, anomalous southerly flow over the western North Pacific associated with a weak Aleutian low enhances the moisture flux into coastal Asia, in agreement with the precipitation signal there. The weak amplitude of the precipitation anomalies over the western United States in the earliest epoch difference map compared to the later ones may be related to the lack of an appreciable SLP signal over the eastern North Pacific in the former.

The time series of the precipitation difference between Alaska (55°–60°N, 160°–135°W) and Japan (32.5°–47.5°N, 130°–146°E) is shown in Fig. 4 together with the NPI. The precipitation record exhibits a high degree of similarity to the NPI; their correlation coefficient is 0.66 based upon data smoothed with a three-point binomial filter and is a maximum at 0 lag. The interdecadal regimes evident in the NPI are also apparent in the precipitation difference record, demonstrating the impact of large-scale atmospheric circulation variations upon climate on both sides of the Pacific.

Figure 5 shows epoch difference maps for winter air temperature and SLP. Interior Alaska and northwestern Canada are cold when the Aleutian low is weak, consistent with the results of Minobe (1997) based upon individual station records. The western North Pacific Ocean, on the other hand, is relatively warm, mainly in the region of reduced westerly wind strength, consistent with an equilibrated response to the underlying SST change (Fig. 6) due to diminished upward turbulent energy fluxes at the sea surface and cold advection by anomalous Ekman currents (cf. Miller et al. 1994). The time series of air temperature over Alaska and northwestern Canada (51°–70°N, 175°–100°W) is shown in Fig. 4. Like the precipitation difference record, it exhibits strong support for the interdecadal regimes evident in the NPI; the correlation coefficient between the air temperature record and the NPI is 0.74 based upon data smoothed with a three-point binomial filter and is maximum at 0 lag.

Epoch difference maps for SST based upon the extended winter season, January–May, are shown in Fig. 6. We use the extended winter season for SST in view of the fact that the correlation between the leading principal component time series of monthly SST anomalies over the North Pacific [termed the Pacific (inter) decadal oscillation (PDO) by M97], and the winter NPI is strongest during these months (not shown). This result is consistent with the notion that the response time for extratropical SST anomalies to atmospheric forcing is on the order of 1 month (Frankignoul 1985; Deser and Timlin 1997) and that once created, SST anomalies persist for many months due to the thermal inertia associated with a deep winter mixed layer (cf. Deser et al. 2003). However, epoch difference maps based upon December–March look very similar to those based upon the extended winter season (not shown). The SST epoch differences (Fig. 6) exhibit positive values over the central and western Pacific centered along ~40°N and negative values in the eastern and far northern Pacific, similar to the leading EOF of monthly SST anomalies shown in M97. Some differences are apparent between the first and last epoch difference maps, particularly in the Gulf of Alaska, where negative values are found in the early one and positive values in the later one. Note the overall similarity between the SST and marine air temperature patterns shown in Fig. 5.

The January–May PDO record (obtained online at http://tao.atmos.washington.edu/pdo) is shown in Fig. 4. This time series exhibits a greater proportion of interdecadal compared to interannual variability than do the atmospheric indices shown in the figure, consistent with the greater thermal inertia of the ocean mixed layer compared to the atmosphere (cf. Frankignoul and Hasselmann 1977; Deser et al. 2003). With the exception of the first decade of the twentieth century, the SST record is highly coherent with each of the atmospheric indices; the correlation coefficient between the PDO record and the NPI is 0.64 (maximum at zero lag; 0.78 for the period 1911–97). The origin of the discrepancy between the SST and atmospheric records during the first decade of the twentieth century requires further study; however, it is unlikely that the atmospheric re-

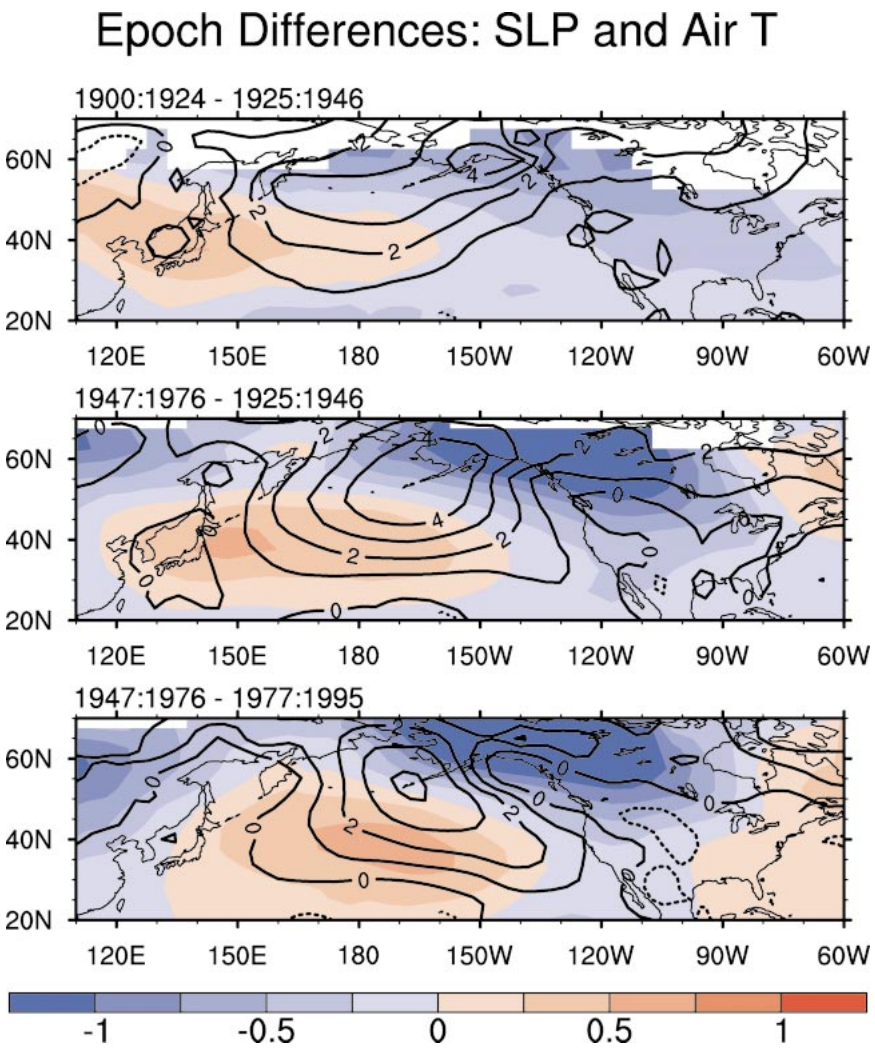

FIG. 5. As in Fig. 3 but for winter SLP (contours) and surface air temperature (color shading). The air temperature scale (color bar at bottom of figure) is in units of °C.

cords are erroneous in light of their mutual consistency. More likely, in our view, is that the SST index contains spurious signals due to the paucity of data during this period, a speculation that deserves further investigation. The 1925 and 1947 climate transitions in the NPI appear to be preceded by shifts in the PDO index by a couple of years. We caution against attaching too much significance to this apparent lead of the ocean relative to the atmosphere since 1) the 1977 transition is simultaneous and 2) the NPI and PDO correlate most strongly at 0 lag (not shown).

b. Tropical linkages

1) SST

To identify areas in the Tropics where SSTs vary coherently with the NPI on time scales longer than interannual, we show in Fig. 7 the correlation map between the NPI and boreal winter SST anomalies based upon the period 1900–97 using low-pass-filtered data to emphasize fluctuations with periods greater than ~9 yr (the results are not unduly sensitive to the low-pass filter used, provided that the cutoff is at periods longer than a few years). The strongest positive correlations ($r >$ 0.6) are found in the tropical Indian Ocean extending into the far western Pacific and outside of the equatorial zone in the eastern tropical Pacific. The correlations within the Indian Ocean reach peak values of 0.8 along ~10°N. Weak and insignificant correlations are found along the equator east of 180°.

Another view of the SST anomaly patterns associated with interdecadal variations in the NPI is obtained from epoch difference maps based on Kaplan et al. (1998) data (Fig. 8, left). Negative values are found over most of the tropical Indo-Pacific in all three epoch differences except for weak positive values along the equator be-

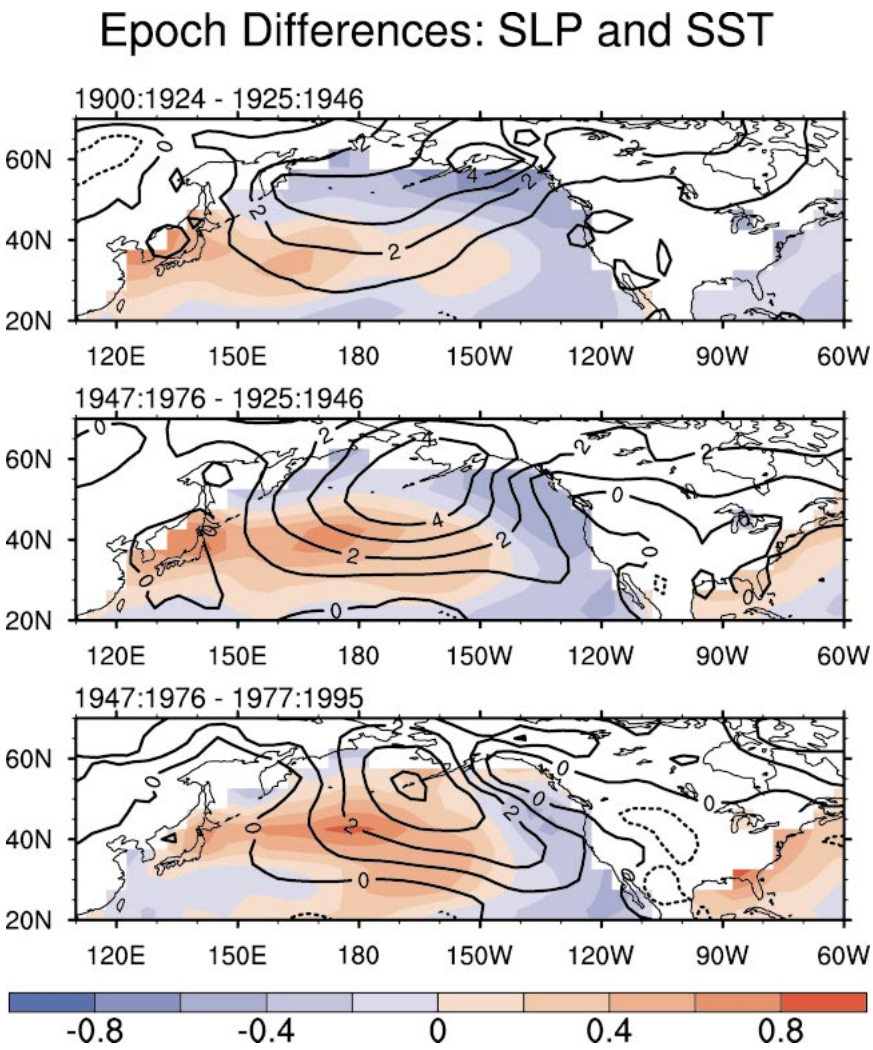

FIG. 6. As in Fig. 3 but for winter SLP (contours) and winter–spring (Dec–Mar) SST (color shading). The SST scale (color bar at bottom of figure) is in units of °C.

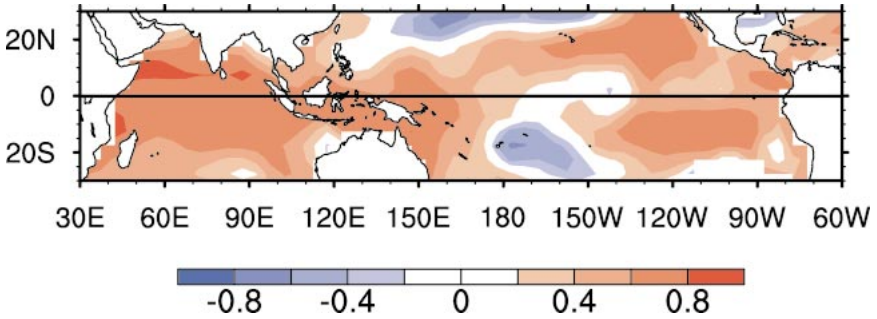

FIG. 7. Correlation map between the inverted NPI and boreal winter SST anomalies in the tropical Indo-Pacific, based on 9-yr low-pass-filtered data during the period 1900–97. The color bar shows the scale for the correlation coefficients.

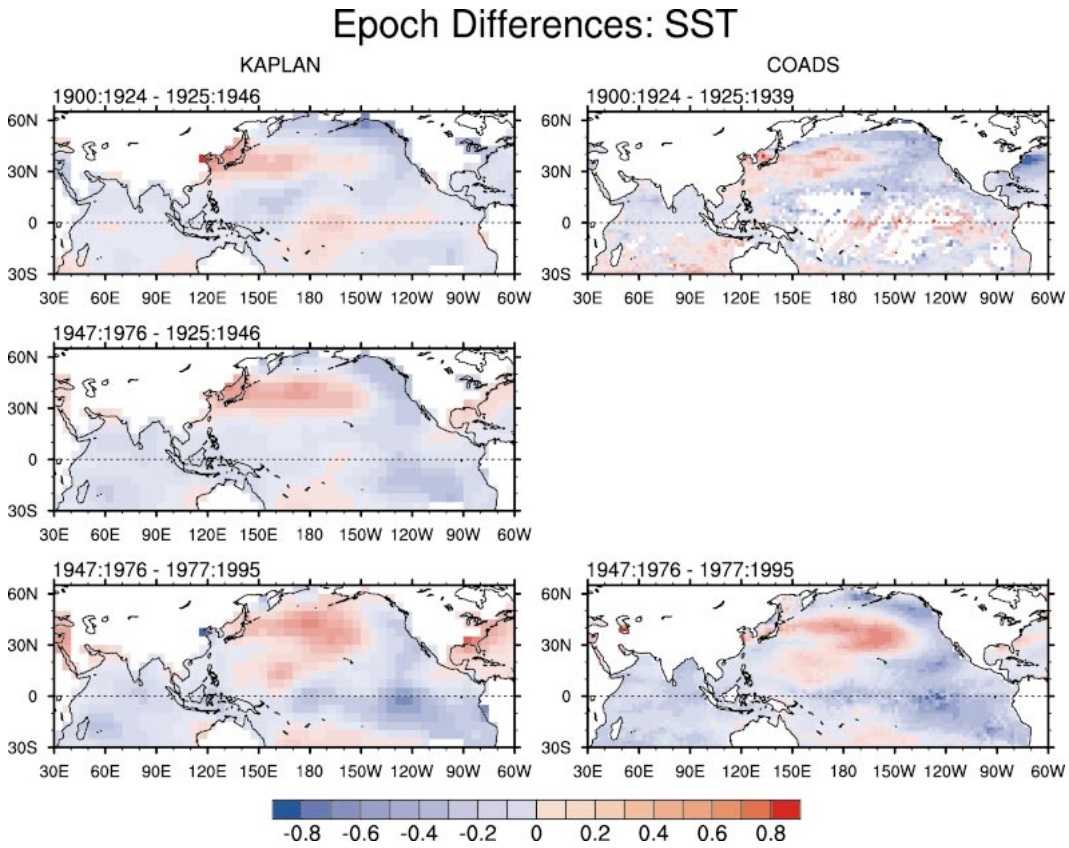

FIG. 8. Epoch difference maps of boreal winter SST from (left) the Kaplan et al. (1998) dataset and (right) COADS. The scale (color bar at bottom of figure) is in units of °C. Note that the COADS data are not interpolated (white areas denote missing data). The middle panel has been omitted for COADS due to the artificial increase in SSTs between 1940 and 1941 resulting from a change in observing practice. For the same reason, the earliest epoch difference map based upon (top right) COADS excludes data from the period 1940–46.

tween the international date line and the coast of South America in the earliest one. Note that although the magnitudes of the SST differences in the Indian Ocean are relatively small (~0.2 K), they are highly significant statistically due to the relatively weak background interannual variability. The opposing sign of the equatorial east Pacific ''cold tongue'' SST anomalies between the first and last epoch differences results in weak correlations with the NPI for the twentieth century as a whole (recall Fig. 7). Other seasons also exhibit weak positive values in the eastern equatorial Pacific for the earliest epoch difference (not shown). The COADS (Fig. 8, right) confirms the results based upon Kaplan et al. (1998), indicating that this feature is not due to the way in which the Kaplan et al. SST data were processed (recall section 2). Further support for the credibility of the change in sign of the SST anomalies in the equatorial cold tongue between the first and last epoch differences is the similar behavior of SLP anomalies at Darwin, Australia (not shown), a reliable index of the Southern Oscillation (cf. Wright et al. 1988; Deser and Wallace 1990). Indeed, the Darwin SLP record correlates with the cold tongue SST index (CTI; SST anomalies averaged over the region 5°N–5°S, 180°–110°W; see Deser and Wallace 1990) at a level of 0.87 based upon averages for boreal winter during 1900–46 (0.85 during 1947–97), attesting to the fidelity of both records.

Figures 7 and 8 indicate that SST fluctuations in the tropical Indian Ocean and the eastern Pacific north and south of the equator are associated with low-frequency variations in the NPI. The SST anomaly time series for the tropical Indian (10°S–20°N, 50°–125°E) and southeast tropical Pacific (5°–20°S, 140°–90°W) are shown in Fig. 9, together with the NPI (the northeast tropical Pacific is similar to the southeast record, but is less highly correlated with the NPI, and the interdecadal regimes are less pronounced; not shown). Both records correspond well with the NPI, with correlations of 0.67 and 0.65, respectively, based upon data smoothed with a three-point binomial filter (the correlations are a maximum at 0 lag). The interdecadal regimes evident in the NPI are apparent in the tropical SST time series except for the early portion of the first epoch in the southeast Pacific record.

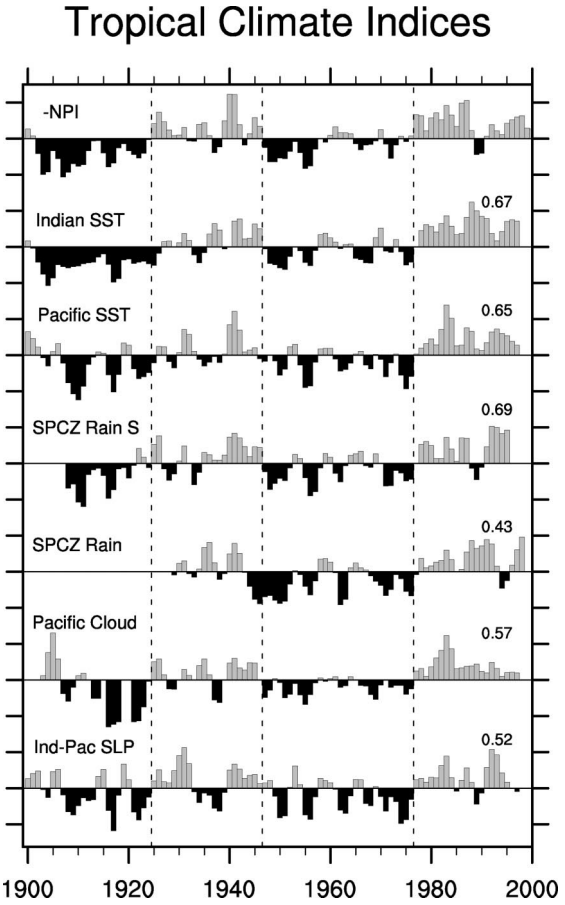

FIG. 9. Selected regional climate anomaly records over the tropical Indo-Pacific for boreal winter during 1900–97: the inverted NPI (through 2000), tropical Indian Ocean SST, southeast tropical Pacific SST, rainfall south of the SPCZ, rainfall within the SPCZ, central Pacific cloudiness, and tropical Indian Ocean minus southeast Pacific SLP. Regions are defined in the text and shown in Figs. 11–13. All records are normalized and smoothed with a three-point binomial filter. Each tick mark on the ordinate represents one std dev. The numeral to the right of each tropical index represents its correlation coefficient with the inverted NPI.

2) PRECIPITATION

Although SST changes over the tropical Indian and southeastern tropical Pacific Oceans are coherent with interdecadal variations in the NPI, SST anomalies per se do not force atmospheric teleconnections to higher latitudes; the release of latent heat in precipitating deep convection is the direct forcing mechanism. Therefore, we examine the tropical rainfall changes associated with interdecadal variations in the NPI using station data over land and cloudiness as a proxy over the oceans. As background to the epoch difference maps, the long-term mean precipitation distribution during boreal winter based upon satellite measurements (Xie and Arkin 1997) for the period 1979–97 is shown in Fig. 10 (top). The highest rainfall amounts occur over the southwestern tropical Pacific within the South Pacific convergence zone (SPCZ), along ~7°N within the Pacific Intertropical convergence zone (ITCZ), and over the equatorial Indian Ocean, with maximum values (>12 mm day^{-1}) near 10°S, 170°E. The long-term mean cloud amount distribution from COADS for the same period is shown in Fig. 10 (bottom). In general, the regions of high rainfall correspond to areas of high total cloud cover (values >5 octas). In addition, large cloud amounts occur west of North and South America and west of Australia, areas dominated by shallow nonprecipitating clouds (Klein and Hartmann 1993), and poleward of 30°N.

Epoch difference maps for land station precipitation are shown in Fig. 11. Coherent rainfall changes are evident in the Tropics where data exist. In the most recent epoch difference, negative values are found within and equatorward of the mean axis of the SPCZ and within the ITCZ over the central Pacific, and positive values obtain on the poleward flanks of the SPCZ and ITCZ (the latter extends westward to the southern tip of India). Over South and Central America, negative values are found between 0° and 20°S, and positive values are found between 0° and 15°N. Positive values are evident in the Hawaiian Islands. The middle epoch difference is similar to the latest one except for the region between southern India and the Philippines where values are near zero. Data coverage in the earliest epoch difference is severely limited, but positive values are still evident over the western Pacific, in keeping with the two later maps. However, stations from the southern tip of India eastward to the Philippines exhibit strongly negative values in the earliest epoch difference, in contrast to the positive values found in the recent epoch difference.

We formed two regional precipitation indices for the tropical western Pacific, choosing areas with consistent signals in all three epoch difference maps (see Fig. 11 for regional outlines); these indices are shown in Fig. 9. The precipitation index for the poleward flank of the SPCZ (''SPCZ Rain S'') is highly correlated with the NPI ($r = 0.69$) and exhibits clear evidence of regime transitions in 1947 and 1977, while the 1925 transition occurred a couple of years in advance (note that this index extends back to 1908 only). The precipitation index for the main branch of the SPCZ (''SPCZ Rain''), which extends back to 1929 only, also shows coherent behavior with the NPI ($r = 0.43$), although the 1947 transition occurred several years too early.

3) MARINE CLOUDINESS

To extend the tropical rainfall analysis to oceanic areas where direct measurements are lacking, we employ reports of total cloudiness from COADS as qualitative proxy records of precipitation. Figure 12 shows a side-by-side comparison of the epoch difference maps for land-based precipitation and ship-based cloudiness in the Tropics during December–March. In regions dominated by deep convective clouds such as the convergence zones, we expect a correspondence between precipitation and cloud cover; in areas where nonprecipi-

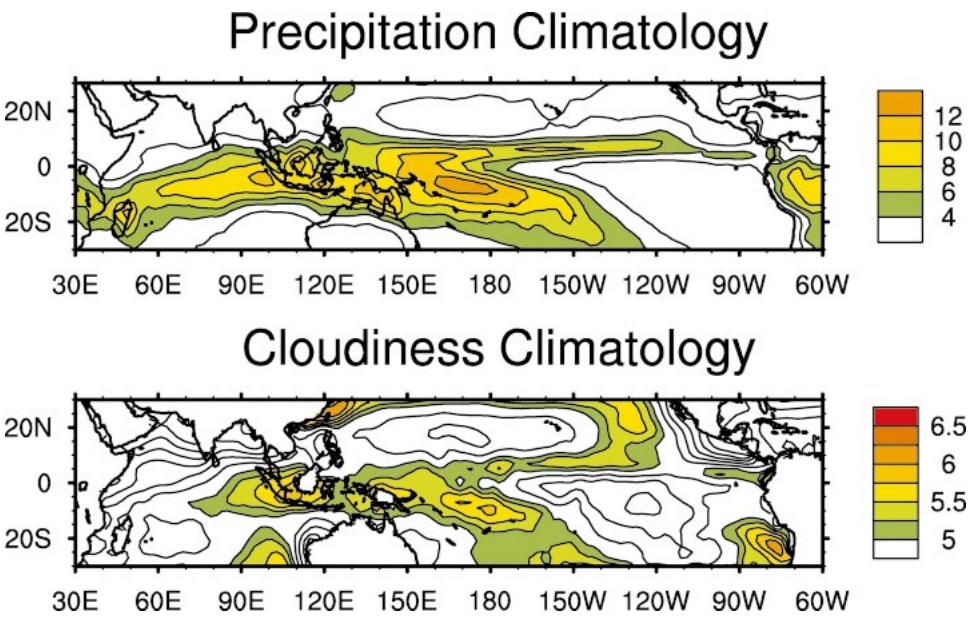

FIG. 10. (top) Climatological distribution of boreal winter precipitation (mm day^{-1}) based upon satellite measurements during the period 1979–97. The contour interval is 2 mm day^{-1}, with values exceeding 4 mm day^{-1} shaded (see color bar at right). (bottom) Climatological distribution of total cloud amount (octas) over the oceans during boreal winter based upon COADS during 1979–97. The contour interval is 0.5 (0.25) octas for values less than (greater than) 5 octas, with values exceeding 5 octas shaded (see color bar at right).

tating (e.g., low stratiform) clouds prevail, such as off the west coasts of South and North America, no such correspondence is expected. The epoch difference maps of marine cloudiness generally support and extend the land-based rainfall results. In particular, reduced cloudiness over the central equatorial Pacific and enhanced cloudiness over the western equatorial Pacific and along the poleward flank of the SPCZ in the two recent maps corroborate the station rainfall changes. The enhanced cloud cover over the western Pacific extends into the eastern Indian Ocean. Increased cloudiness is also found over the eastern tropical Pacific and west of Australia, regions dominated by low-stratiform cloudiness. Positive cloudiness values in the vicinity of the Hawaiian Islands corroborate the land-based rainfall measurements.

The earliest epoch difference is noisier than the other two due to reduced data coverage. Nonetheless, many of the same patterns are discernible, including the oppositely signed anomalies on either side of the equator in the central Pacific, some evidence of enhanced cloud cover over the eastern tropical Pacific, and increased cloudiness over the equatorial Indian Ocean. Diminished cloudiness is found over Indonesia and the South China Sea, roughly consistent with the land-based rainfall results.

The time series of the difference between cloudiness anomalies north and south of the equator in the central Pacific (regions are outlined in Fig. 12) is shown in Fig. 9. This cloudiness index is well correlated with the NPI ($r = 0.57$) and exhibits the regime transitions of 1925, 1947, and 1977. Only the first few years of the record (1903–06; data are missing before 1903) are inconsistent with the NPI (but consistent with the southeastern tropical Pacific SST index).

4) SLP

Epoch difference maps for SLP are shown in Fig. 13. The tropical mean anomaly (25°N–25°S) has been removed from each grid box to enhance the zonal asymmetries. The most recent epoch difference exhibits below-normal values over the Indian and western Pacific Oceans, and above-normal values over the eastern two-thirds of the Pacific, reminiscent of the spatial pattern associated with the Southern Oscillation (cf. Trenberth and Caron 2000). The middle epoch difference is generally similar to the later one, except over the northern Indian Ocean and South China Sea, where positive values are found in place of negative ones. Although noisier due to reduced data coverage, the early epoch difference resembles the middle one with the notable exception of the area around Australia (~10°–20°S, 115°–170°E), where positive values are found in place of negative ones. Thus, the eastern pole of the Southern Oscillation appears to extend considerably farther west in the early epoch difference compared to the later ones, consistent with the Darwin (12°S, 131°E) SLP record discussed above.

Taking into account the nonstationarity of the SLP

patterns, we formed an index of the difference in SLP between the southeastern tropical Pacific (7°–29°S, 167°–89°W) and south Indian (7°–29°S, 57°–129°E) Oceans. Note that this index differs from the canonical SOI, conventionally defined as the SLP difference between Darwin (12°S, 131°E) and Tahiti (17°S, 149°W) or regional averages centered around these stations (cf. Deser and Wallace 1990). The new SLP index, shown as the last record in Fig. 9, correlates well with the NPI ($r = 0.52$) and exhibits ''regime transitions'' in 1925 and 1977 (another shift occurs in 1945, two years before that in the NPI). However, the SLP record is positive during 1900–06, in disagreement with the NPI and the Indian Ocean SST index but consistent with the central Pacific cloud and southeastern tropical Pacific SST time series.

5) An optimal tropical index

Figure 9 provides collective evidence for a robust tropical linkage to North Pacific interdecadal climate variations during boreal winter based upon a diverse set of independent parameters spanning a broad region of the Indo-Pacific. To summarize the suite of tropical climate records shown in Fig. 9, we computed the leading EOF of the six normalized time series (note that the NPI is not included in the EOF analysis). The leading principal component (PC) time series, which accounts for 64% of the variance compared to 16% for the second PC, is shown in Fig. 14 together with the NPI (the six input time series contribute nearly equally to the leading EOF). All three regime transitions evident in the NPI (1925, 1947, and 1977) are present in the leading PC of the tropical records. The correlation coefficient between the two time series is 0.72, based upon data smoothed with a three-point binomial filter; that is, half of the variance of the NPI at periods longer than ~3 yr is coherent with the leading tropical PC time series.

Power spectra of the detrended NPI and the leading tropical PC time series are shown in Fig. 15. Both spectra exhibit enhanced variance at the lowest frequencies (periods > ~20 yr) and a deficit of power around 8–14 yr. The tropical PC power spectrum also exhibits an enhancement of power at interannual frequencies (~4–7 yr). The increased power at interdecadal periods in both records is significant at the 95% confidence level based upon a first-order autoregressive model null hypothesis. The cross-spectrum between the two records (Fig. 15, bottom) exhibits high squared coherence (~0.8) at periods >20 yr and between 4 and 7 yr [values exceeding 0.6 (0.75) are statistically significant at the 95% (99%) confidence level].

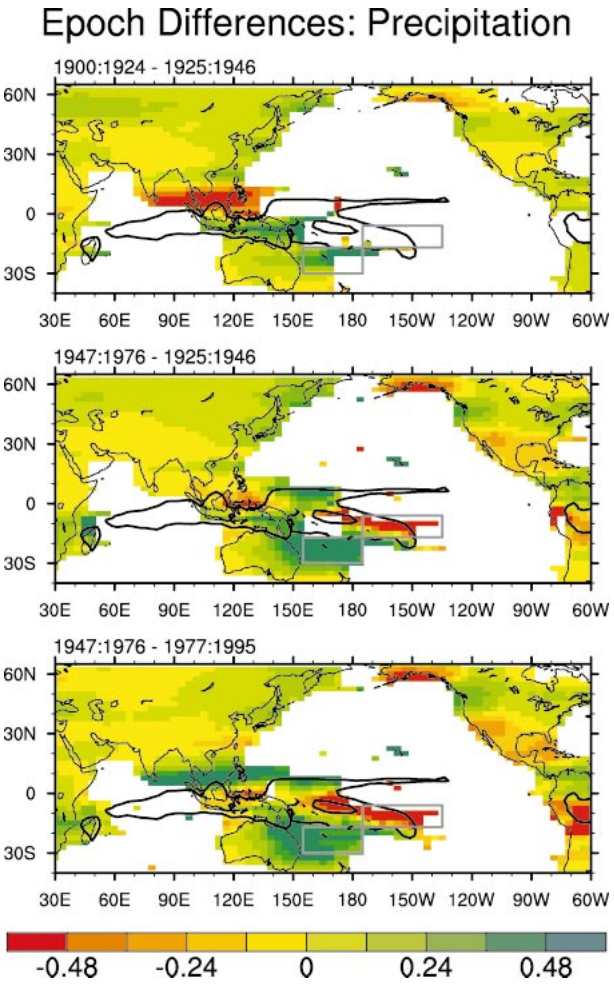

FIG. 11. Epoch difference maps of boreal winter precipitation over land. The precipitation scale (color bar at bottom of figure) is in units of mm day^{-1}. The black contours denote the 7.5 and 12 mm day^{-1} contours from the climatology. Rectangles outline regions used for the time series shown in Fig. 9.

4. Discussion

The earliest epoch difference (1900–24 minus 1925–46) exhibits some notable distinctions from the later two (1947–76 minus 1925–46 and 1947–76 minus 1977–97), including a change in the sign of the SST anomalies in the equatorial Pacific cold tongue, a westward shift (~50° of longitude) of the nodal line between positive and negative SLP anomalies such that Darwin, Australia is no longer located within the western pole of the Southern Oscillation, and a change in the sign of the rainfall/cloudiness anomalies over Borneo, the Philippines, and the South China Sea. These differences highlight that with only three realizations of interdecadal variability to study, it is problematic to characterize any single case as ''canonical.'' These differences also underscore that conventional ENSO indices such as the Darwin SOI and CTI fail as robust metrics of the interdecadal variability. Specifically, neither Darwin SLP nor the CTI exhibit regime transitions in 1925 and 1947 that characterize the NPI, although they do portray the 1977 shift (Fig. 16; note that the Darwin SOI and CTI records in this figure differ from the versions of the SOI

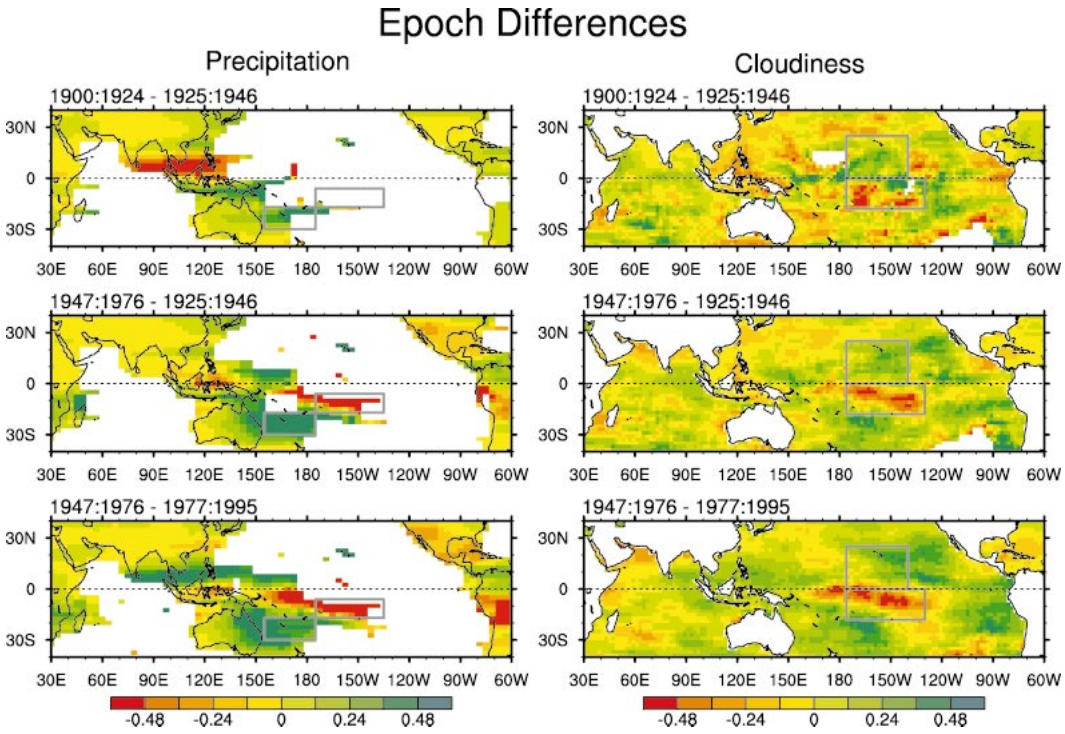

FIG. 12. As in Fig. 11 but for (left) land station precipitation and (right) marine cloudiness. The cloudiness (precipitation) color bar is in units of octas (mm day^{-1}). Rectangles outline regions used for the time series shown in Fig. 9.

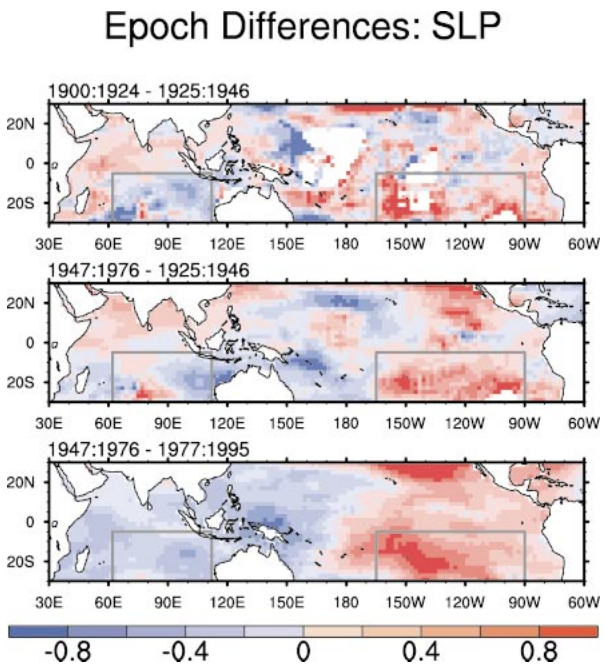

FIG. 13. As in Fig. 11 but for boreal winter SLP. The SLP color bar is in units of hPa. Rectangles outline regions used for the time series shown in Fig. 9.

and CTI shown in Fig. 2 from M97). With regard to the change in sign of the rainfall anomalies over the region encompassing Borneo, the Philippines, and the South China Sea between the early and recent epoch differences, it is interesting to note that this change coincides with an alteration of the SLP anomaly signal over the eastern North Pacific (recall Fig. 3); whether the two are causally related remains to be elucidated.

Given the evidence for a tropical Indo-Pacific linkage to interdecadal climate variations over the North Pacific, it is natural to inquire whether there are any distinctions between these connections and those that occur in as-

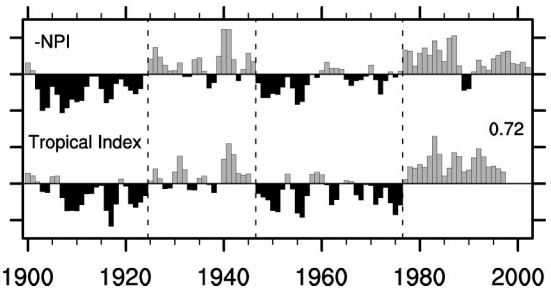

FIG. 14. (top) The inverted NPI and (bottom) the optimal tropical index (see text for definition) during 1900–97. Both records have been normalized and smoothed with a three-point binomial filter. Each tick mark on the ordinate represents 1 std dev. The numeral to the right of the tropical index represents its correlation coefficient with the inverted NPI.

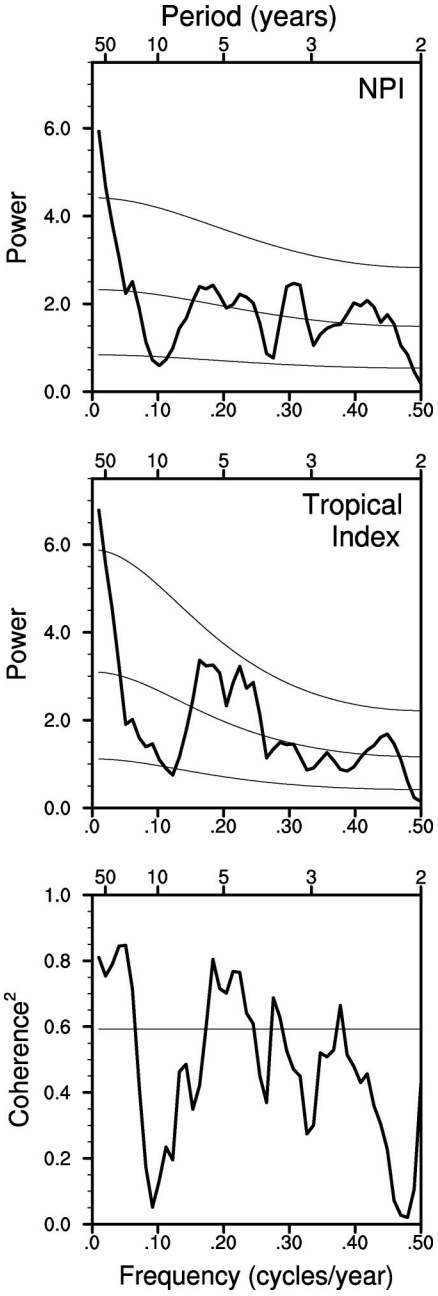

FIG. 15. Power spectra of (top) the NPI and (middle) the optimal tropical index based upon detrended data for the period 1900–97 (thick curves). The thin curves represent the power spectrum and its 95% confidence limits for a ''red noise'' null hypothesis based upon a first-order autoregressive process with the same autocorrelation as the observed time series (0.21 for the NPI and 0.32 for the tropical index). (bottom) Squared coherence between the NPI and the tropical index (thick curve). The 95% confidence level is 0.6 (thin horizontal line).

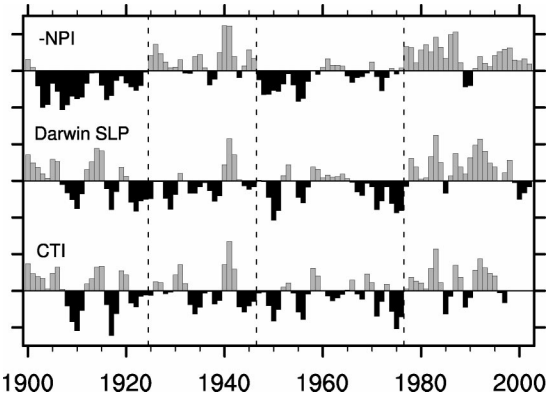

FIG. 16. (top) The inverted NPI, (middle) Darwin SLP, and (bottom) eastern equatorial Pacific SST (the CTI) records during 1900–2002 (1900–97 for the CTI). All records are for boreal winter and have been normalized and smoothed with a three-point binomial filter. Each tick mark on the ordinate represents one std dev.

sociation with the interannual ENSO cycle. Figure 17 shows a comparison of the ENSO and interdecadal patterns of SST and cloudiness anomalies during boreal winter. The ENSO patterns were obtained by regressing the anomaly fields upon the CTI during 1947–97, and the interdecadal patterns are those associated with the 1977 transition. The two SST anomaly patterns (Fig. 17, top) are broadly similar, with positive values throughout much of the tropical Indian and Pacific Oceans and a dipole pattern in the North Pacific with positive values in the east and negative values in the center. Some differences are also apparent, however; compared to ENSO, the epoch difference is characterized by a more equal weighting of the tropical Indian and Pacific anomalies, a broader meridional extent of the eastern equatorial Pacific anomalies, and a more equal weighting between the North Pacific and the Tropics. These results are in agreement with the findings of Garreaud and Battisti (1999) based upon annual averages. However, note that in the earliest epoch difference, the SST anomalies along the equatorial upwelling zone are opposite in sign to those associated with ENSO (recall Fig. 8).

The interdecadal and ENSO anomaly patterns of total cloud amount (Fig. 17, bottom) are also similar, with enhanced cloud cover over the western and central equatorial Pacific and diminished cloudiness over the far western Pacific and the far eastern Indian Ocean. Reduced cloud cover is also found in the stratus regions of the eastern tropical Pacific in association with a warmer sea surface. We note that the stratus cloud signal is relatively more pronounced in the epoch difference than in the ENSO regression map; the reasons for this require further study. The ENSO cloudiness regression pattern is consistent with the results of Park and Leovy (2004).

The short duration of the instrumental records limits our ability to assess whether the interdecadal variability sampled during the twentieth century is indicative of a preferred time scale or is part of a continuum of low-frequency variability. Paleoclimate proxies based upon climatically sensitive biological indicators are better

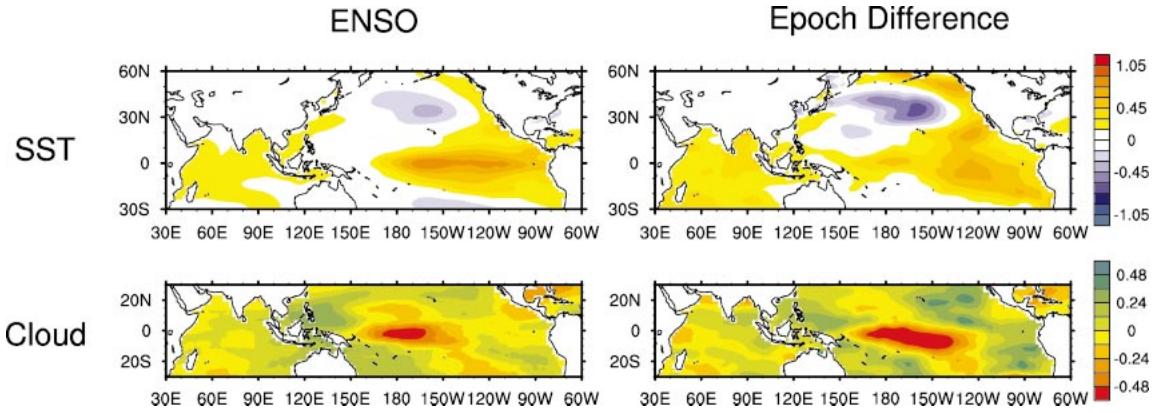

FIG. 17. Comparison between (left) ENSO and (right) epoch difference patterns of (top) SST and (bottom) cloudiness anomalies during boreal winter. The ENSO patterns are based upon linear regression of the anomaly fields upon the CTI during 1947–97, and the epoch difference maps are obtained by subtracting the period 1947–76 from the period 1977–97. The color bar scale for the SST (cloudiness) anomalies is given on the rhs of the figure in units of °C (octas). Note that the ENSO-related anomalies are per unit std dev of the CTI.

suited for addressing the issue of time scale due to their longer record lengths. Recently, Cole et al. (2000) presented a 194-yr record (1804–1994) of skeletal δ^{18}O from a coral growing in the far western tropical Indian Ocean at Malindi Marine Park, Kenya (3°S, 40°E). According to Cole et al. (2000), this record primarily reflects fluctuations in SST as opposed to salinity. The detrended δ^{18}O time series is shown together with the leading tropical PC index in Fig. 18 (top). Interdecadal variations in δ^{18}O are present during both centuries, and those during the twentieth century are coherent with the instrumental record (the correlation coefficient between the δ^{18}O and PC time series is 0.62 based upon data smoothed with a three-point binomial filter). The power spectrum of the δ^{18}O record (Fig. 18, bottom) exhibits a large proportion of variance at periods longer than ~30 yr, with relatively little variance at higher frequencies. The predominantly low-frequency character of the δ^{18}O time series is reflected in the high year-to-year autocorrelation (0.64), a value considerably larger than that for nearby SST anomalies or the tropical PC record (~0.3). The higher persistence in the δ^{18}O record may be partly biological in nature and/or due to the way in which it was decimated to annual values (see Cole et al. 2000). Despite its duration, even the 194-yr δ^{18}O record is not sufficiently long to assess whether the enhanced variance at low frequencies is indicative of a well-defined (albeit broadband) spectral peak at interdecadal periods or whether it reflects a red noise process with no preferred time scale.

Although the Indian Ocean coral record shows a favorable match to the instrumental time series and provides evidence that the interdecadal fluctuations continue back at least 200 yr, other proxy records such as tree ring chronologies from North and South America are not as consistent in their behavior during the nineteenth century (Villalba et al. 1999). The lack of agreement among the proxy records suggests the need for additional paleoclimate indicators at key locations of Pacific interdecadal variability. One such location suggested by our study is the tropical Indian and western Pacific Oceans for both SST and precipitation-sensitive proxies.

5. Summary and interpretation

The analyses presented in this study support the notion that interdecadal fluctuations in the winter NPI during the twentieth century are associated with climate variations over the tropical Indo-Pacific, in agreement with earlier studies (e.g., M97; Minobe 1997; Zhang et al. 1997; Garreaud and Battisti 1999). Specifically, SSTs in the tropical Indian and southeastern Pacific Oceans, rainfall and cloudiness along the SPCZ and over the central equatorial Pacific, cloudiness over the eastern tropical Pacific, and the SLP difference between the tropical southeast Pacific and Indian Oceans collectively exhibit variability that is coherent with the NPI on interannual and interdecadal time scales. This study has extended our knowledge of Pacific interdecadal climate variability by considering a more comprehensive suite of climatic parameters in the tropical Indo-Pacific than in previous studies and by focusing upon the relationships during boreal winter when the NPI is most active and the influence of the tropical Indo-Pacific upon the atmospheric circulation over the North Pacific is well established. In addition, our case study approach has allowed for an assessment of the similarities and differences among the three cases of interdecadal variability sampled in the twentieth-century observational record.

Our interpretation of the results is that variations in the winter NPI at periods ranging from interannual to interdecadal represent, in part, a remote response to rainfall anomalies over the tropical western and central Pacific via dynamical atmospheric teleconnection processes. A similar hypothesis is implicit in the recent study of Newman et al. (2003; see also Trenberth and Hurrell 1994), although their metric of tropical forcing

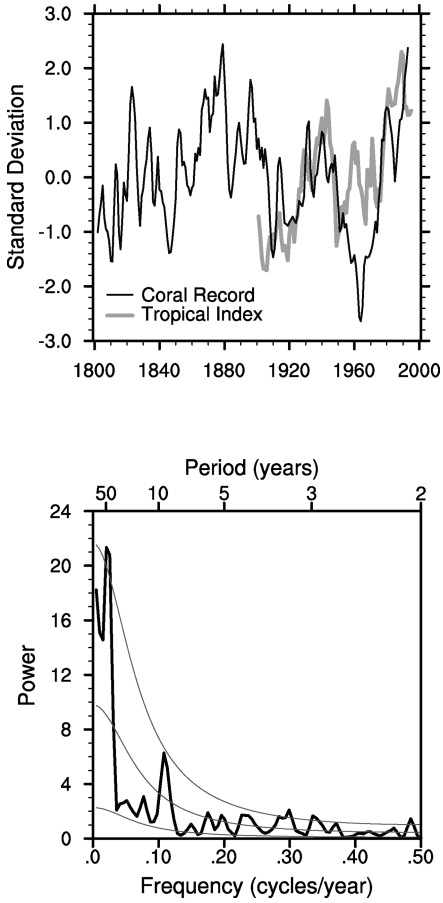

FIG. 18. (top) Time series of the detrended inverted δ^{18}O coral record from the western Indian Ocean (thin black curve; Cole et al. 2000) and the instrumental tropical index (thick gray curve). Both time series have been normalized by their std dev, and the coral record (tropical index) was smoothed with a three-point (five-point) binomial filter to facilitate visual comparison. (bottom) Power spectrum of the δ^{18}O coral record based upon detrended data for the period 1801–1994. The thin curves represent the power spectrum and its 95% confidence limits for a red noise null hypothesis based upon a first-order autoregressive process with the same autocorrelation as the observed time series (0.64).

does not capture the full amplitude of the observed interdecadal variability evident in our ''optimal tropical index.'' Note that our interpretation does not preclude a feedback role for atmospherically induced SST anomalies within the North Pacific that may serve to amplify and/or ''redden'' the SLP response to tropical forcing, for example, through the large-scale dynamical atmospheric circulation response to North Pacific SST anomalies (Peng et al. 1997) or the mechanism of ''reduced thermal damping'' (Bretherton and Battisti 2000; Alexander et al. 2002) associated with the thermal inertia of the deep winter ocean mixed layer (Alexander and Deser 1995; Deser et al. 2003). Nor does it preclude the existence of feedbacks from the North Pacific to the Tropics via an atmospheric bridge (e.g., Barnett et al. 1999; Vimont et al. 2001) and/or an oceanic one (e.g., Klecman et al. 1999; Zhang and McPhaden 2002). Indeed, these feedbacks may be essential for explaining the origin of the interdecadal climate variations within the tropical Indo-Pacific, a question not addressed in the present study and one that remains outstanding.

Acknowledgments. We wish to acknowledge helpful discussions with many colleagues, including Drs. M. Alexander, D. Battisti. M. Newman, K. Trenberth, and J. M. Wallace. The comments of the editor and two anonymous reviewers helped us to improve the presentation of the results. This work was supported by a grant from NOAA's Office of Global Programs to C. Deser and J. Hurrell.

REFERENCES

Alexander, M. A., and C. Deser, 1995: A mechanism for the recurrence of wintertime midlatitude SST anomalies. *J. Phys. Oceanogr.,* **25,** 122–137.

——, I. Blade, M. Newman, J. R. Lanzante, N.-C. Lau, and J. D. Scott, 2002: The atmospheric bridge: The influence of ENSO teleconnections on air–sea interaction over the global oceans. *J. Climate*, **15,** 2205–2231.

Barnett, T. P., D. W. Pierce, M. Latif, D. Dommenget, and R. Saravanan, 1999: Interdecadal interactions between the Tropics and midlatitudes in the Pacific basin. *Geophys. Res. Lett.,* **26,** 615–618.

Bretherton, C., and D. S. Battisti, 2000: An interpretation of the results from atmospheric general circulation models forced by the time history of the observed sea surface temperature distribution. *Geophys. Res. Lett.,* **27,** 767–770.

Cayan, D. R., S. A. Kammerdiener, M. D. Dettinger, J. M. Caprio, and D. H. Peterson, 2001: Changes in the onset of spring in the western United States. *Bull. Amer. Meteor. Soc.,* **82,** 399–415.

Chao, Y., M. Ghil, and J. C. McWilliams, 2000: Pacific interdecadal variability in this century's sea surface temperatures. *Geophys. Res. Lett.*, **27,** 2261–2264.

Cole, J. E., R. B. Dunbar, T. R. McClanahan, and N. A. Muthiga, 2000: Tropical Pacific forcing of decadal SST variability in the western Indian Ocean over the past two centuries. *Science,* **287,** 617–619.

Deser, C., and J. M. Wallace, 1990: Large-scale atmospheric circulation features of warm and cold episodes in the tropical Pacific. *J. Climate,* **3,** 1254–1281.

——, and M. S. Timlin, 1997: Atmosphere–ocean interaction on weekly timescales in the North Atlantic and Pacific. *J. Climate,* **10,** 393–408.

——, M. A. Alexander, and M. S. Timlin, 1996: Upper-ocean thermal variations in the North Pacific during 1970–1991. *J. Climate,* **9,** 1840–1855.

——, ——, and ——, 2003: Understanding the persistence of sea surface temperature anomalies in midlatitudes. *J. Climate,* **16,** 57–72.

Dettinger, M. D., D. R. Cayan, G. M. McCabe, and J. A. Marengo, 2000: Multiscale streamflow variability associated with El Niño/Southern Oscillation. *El Niño and the Southern Oscillation—Multiscale Variability and Global and Regional Impacts,* H. F. Diaz and V. Markgraf, Eds., Cambridge University Press, 113–146.

Folland, C. K., and D. E. Parker, 1995: Correction of instrumental biases in historical sea surface temperature data. *Quart. J. Roy. Meteor. Soc.,* **121,** 319–367.

Frankignoul, C., 1985: Sea surface temperature anomalies, planetary waves and air–sea feedback in middle latitudes. *Rev. Geophys.,* **23,** 357–390.

——, and K. Hasselmann, 1977: Stochastic climate models. Part 2.

Application to sea-surface temperature variability and thermocline variability. *Tellus,* **29,** 284–305.
——, E. Kestenare, N. Sennéchael, G. de Coëtlogon, and F. D'Andrea, 2000: On decadal-scale ocean–atmosphere interactions in the extended ECHAM1/LSG climate simulation. *Climate Dyn.,* **16,** 333–354.
Garreaud, R. D., and D. S. Battisti, 1999: Interannual and interdecadal variability of the tropospheric circulation in the Southern Hemisphere. *J. Climate,* **12,** 2113–2123.
Graham, N. E., T. P. Barnett, R. Wilde, M. Ponater, and S. Schubert, 1994: On the roles of tropical and midlatitude SSTs in forcing interannual to interdecadal variability in the winter Northern Hemisphere circulation. *J. Climate,* **7,** 1416–1441.
Gu, D. F., and S. G. H. Philander, 1997: Interdecadal climate fluctuations that depend on exchanges between the Tropics and extratropics. *Science,* **275,** 805–807.
Houghton, J. T., L. G. Meira Filho, B. A. Callander, N. Harris, A. Kattenberg, and K. Maskell, Eds., 1996: *Climate Change 1995: The Science of Climate Change.* Cambridge University Press, 572 pp.
Hulme, M., T. J. Osborn, and T. C. Johns, 1998: Precipitation sensitivity to global warming: Comparison of observations with HadCM2 simulations. *Geophys. Res. Lett.,* **25,** 3379–3382.
Jones, P. D., 1994: Hemispheric surface air temperature variations: A reanalysis and an update to 1993. *J. Climate,* **7,** 1794–1802.
Kaplan, A., M. Cane, Y. Kushnir, A. C. Clement, M. B. Blumenthal, and B. Rajagopalan, 1998: Analyses of global sea surface temperature 1856–1991. *J. Geophys. Res.,* **103,** 18 567–18 589.
Kleeman, R., J. P. McCreary, and B. A. Klinger, 1999: A mechanism for generating ENSO decadal variability. *Geophys. Res. Lett.,* **26,** 1743–1746.
Klein, S. A., and D. L. Hartmann, 1993: The seasonal cycle of low stratiform clouds. *J. Climate,* **6,** 1587–1605.
Knutson, T. R., and S. Manabe, 1998: Model assessment of decadal variability and trends in the tropical Pacific Ocean. *J. Climate,* **11,** 2273–2296.
Latif, M., and T. P. Barnett, 1996: Decadal climate variability over the North Pacific and North America: Dynamics and predictability. *J. Climate,* **9,** 2407–2423.
Liu, Z., L. Wu, R. Gallimore, and R. Jacob, 2002: Search for the origins of Pacific decadal climate variability. *Geophys. Res. Lett.,* **29,** 1404, doi:10.1029/2001GL013735.
Mantua, N. J., and S. R. Hare, 2002: The Pacific Decadal Oscillation. *J. Oceanogr.,* **58,** 35–44.
——, ——, Y. Zhang, J. M. Wallace, and R. C. Francis, 1997: A Pacific interdecadal oscillation with impacts on salmon production. *Bull. Amer. Meteor. Soc.,* **78,** 1069–1079.
McPhaden, M. J., and D. Zhang, 2002: Slowdown of the meridional overturning circulation in the upper Pacific Ocean. *Nature,* **415,** 603–608.
Miller, A. J., D. R. Cayan, T. P. Barnett, N. E. Graham, and J. M. Oberhuber, 1994: Interdecadal variability of the Pacific Ocean: Model response to observed heat flux and wind stress anomalies. *Climate Dyn.,* **10,** 287–302.
Minobe, S., 1997: A 50–70 year climatic oscillation over the North Pacific and North America. *Geophys. Res. Lett.,* **24,** 683–686.
Newman, M., G. P. Compo, and M. A. Alexander, 2003: ENSO-forced variability of the Pacific decadal oscillation. *J. Climate,* **16,** 3853–3857.
Nitta, T., and S. Yamada, 1989: Recent warming of tropical sea surface temperature and its relationship to the Northern Hemisphere circulation. *J. Meteor. Soc. Japan,* **67,** 375–383.
Nonaka, M., S.-P. Xie, and J. P. McCreary, 2002: Decadal variations in the subtropical cells and equatorial Pacific SST. *Geophys. Res. Lett.,* **29,** 1116, doi:10.1029/2001GL013717.
Park, S., and C. B. Leovy, 2004: Marine low-cloud anomalies associated with ENSO. *J. Climate,* **17,** 3448–3469.
Peng, S., W. A. Robinson, and M. P. Hoerling, 1997: The modeled atmospheric response to midlatitude SST anomalies and its dependence on background circulation states. *J. Climate,* **10,** 971–987.
Pierce, D. W., T. P. Barnett, N. Schneider, R. Saravanan, D. Dommenget, and M. Latif, 2001: The role of ocean dynamics in producing decadal climate variability in the North Pacific. *Climate Dyn.,* **18,** 51–70.
Robertson, A. W., 1996: Interdecadal variability over the North Pacific in a multi-century climate simulation. *Climate Dyn.,* **12,** 227–241.
Schneider, N., A. J. Miller, M. A. Alexander, and C. Deser, 1999: Subduction of decadal North Pacific temperature anomalies: Observations and dynamics. *J. Phys. Oceanogr.,* **29,** 1056–1070.
Trenberth, K. E., 1984: Some effects of finite sample size and persistence on meteorological statistics. Part I: Autocorrelations. *Mon. Wea. Rev.,* **112,** 2359–2368.
——, and D. A. Paolino Jr., 1980: The Northern Hemisphere sea-level pressure data set: Trends, errors and discontinuities. *Mon. Wea. Rev.,* **108,** 855–872.
——, and J. W. Hurrell, 1994: Decadal atmospheric–ocean variations in the Pacific. *Climate Dyn.,* **9,** 303–319.
——, and J. Caron, 2000: The Southern Oscillation revisited: Sea level pressures, surface temperatures, and precipitation. *J. Climate,* **13,** 4358–4365.
——, G. W. Branstator, D. Karoly, A. Kumar, N.-C. Lau, and C. Ropelewski, 1998: Progress during TOGA in understanding and modeling global teleconnections associated with tropical sea surface temperatures. *J. Geophys. Res.,* **103,** 14 291–14 324.
Villalba, R., R. D'Arrigo, E. R. Cook, G. Wiles, and G. C. Jacoby, 1999: Inter-decadal climate oscillations along the extra-tropical western coasts of the Americas: Evidence from tree rings over the past four centuries. Preprints, *10th Symp. on Global Change Studies,* Dallas, TX, Amer. Meteor. Soc., CD-ROM, P. 1.3.
Vimont, D. J., D. S. Battisti, and A. C. Hirst, 2001: Footprinting: A seasonal connection between the Tropics and mid-latitudes. *Geophys. Res. Lett.,* **28,** 3923–3936.
Woodruff, S. D., R. J. Slutz, R. L. Jenne, and P. M. Steurer, 1987: A comprehensive ocean–atmosphere data set. *Bull. Amer. Meteor. Soc.,* **68,** 521–527.
Wright, P. B., J. M. Wallace, T. P. Mitchell, and C. Deser, 1988: Correlation structure of the El Nino/Southern Oscillation phenomenon. *J. Climate,* **1,** 609–626.
Xie, P., and P. A. Arkin, 1997: Global precipitation: A 17-year monthly analysis based on gauge observations, satellite estimates, and numerical model outputs. *Bull. Amer. Meteor. Soc.,* **78,** 2539–2558.
Zhang, D., and M. J. McPhaden, 2002: Slowdown of the meridional overturning circulation in the upper Pacific Ocean. *Nature,* **415,** 603–608.
Zhang, Y., J. M. Wallace, and D. S. Battisti, 1997: ENSO-like interdecadal variability: 1900–93. *J. Climate,* **10,** 1004–1020.
Zwiers, F. W., and H. von Storch, 1995: Taking serial correlation into account in tests of the mean. *J. Climate,* **8,** 336–351.